NANO-MICRO LETTERS ARTICLE
www.nmletters.org

# Structure and Magnetic Properties of Monodisperse $Fe^{3+}$-doped $CeO_2$ Nanospheres

Sumalin Phokha[1], Supree Pinitsoontorn[1], Santi Maensiri[2,*]

(Received 4 July 2013; accepted 18 September 2013; published online 15 October 2013)

**Abstract:** This work reports the study concerning the structure and magnetic properties of undoped $CeO_2$ and Fe-doped $CeO_2$ ($Ce_{1-x}Fe_xO_2$, $0.01 \leq x \leq 0.07$) nanospheres with diameters of 100∼200 nm prepared by hydrothermal method using polyvinylpyrrolidone (PVP) as surfactant. The prepared samples were studied by using X-ray diffraction (XRD), Raman spectroscopy, transmission electron microscopy (TEM), high-resolution transmission electron microscopy (HRTEM), X-ray absorption near-edge structure (XANES), and vibrating sample magnetometry (VSM). The XRD results showed that Fe-doped $CeO_2$ was single-phased with a cubic structure, and with $Fe^{3+}$ successfully substituting in $Ce^{4+}$ sites. Raman spectra showed a redshift of $F_{2g}$ mode that caused by the Fe doping. The samples of both undoped $CeO_2$ and Fe-doped $CeO_2$ exhibited room temperature ferromagnetism, and the saturated magnetization ($M_s$) increased with increasing Fe content until $x = 0.05$, and then the samples displayed ferromagnetic loops as well as paramagnetic behavior. The roles of $Ce^{3+}$ and $Fe^{3+}$ spin electrons are discussed for the ferromagnetism in the Fe-doped $CeO_2$.
**Keywords:** Cerium oxide; Nanospheres; Dilute magnetic oxide; Ferromagnetism; Oxygen vacancies; XANES

**Citation:** Sumalin Phokha, Supree Pinitsoontorn and Santi Maensiri, "Structure and Magnetic Properties of Monodisperse $Fe^{3+}$-doped $CeO_2$ Nanospheres", Nano-Micro Lett. 5(4), 223-233 (2013). http://dx.doi.org/10.5101/nml.v5i4.p223-233

## Introduction

Oxide-dilute magnetic semiconductors (O-DMSs) are materials that exhibit ferromagnetic (FM) at room temperature (RT) with a Curie temperature above RT. These O-DMSs are also optically transparent and can be used for the development in spintronic devices [1,2]. Sine devices use both the spin and the charge of electrons can be controlled with an external magnetic field. Many studies report that these O-DMSs display RT-FM in transition metals (TMs) doping when grown as thin films [3] or in powder form [4]. The carrier-induced FM mechanism is used to explain the FM in semiconducting oxides. In some systems, these phenomena are results not only on the effect of TM doping but also on defects, especially oxygen vacancies ($V_O$). Oxygen vacancies have been proposed to play an important role in the magnetic origin for O-DMSs. However, the origin of ferromagnetism in O-DMSs is due to the segregation of metallic clusters.

Recently, TM-doped $CeO_2$ has been also reported to exhibit ferromagnetism at and above room temperature [5-11]. Unlike other O-DMSs, $CeO_2$ has a cubic structure with lattice parameter $a = 0.54113$ nm [12] that will facilitate the integration of spintronic devices with advanced silicon microelectronic devices. The $CeO_2$ is often used as oxygen storage media due to its oxygen storage capacity via $Ce^{4+}/Ce^{3+}$ redox cycles [13-15]. Early work on $CeO_2$-based O-DMSs was focused on thin films [5-7] and only a little work has been carried out on powders, bulk, and nanocrystalline form [10-12,16]. Tiwari *et al.* [5] first discovered RT-FM in $Ce_{1-x}Co_xO_{2-\delta}$ ($x \leq 0.05$) films deposited on a $LaAlO_3$ (001) substrate by a pulsed laser deposition (PLD) technique. These

[1]Department of Physics, Faculty of Science, Khon Kaen University, Khon Kaen, 40002 Thailand
[2]School of Physics, Institute of Science, Suranaree University of Technology, Nakhon Ratchasima, 30000 Thailand
*Corresponding author. E-mail: santimaensiri@g.sut.ac.th; santimaensiri@gmail.com

films are transparent in a visible regime and exhibit a very high Curie temperature ($T_C$) ~740-875 K with large magnetic moments of $6.1 \pm 0.2$~$8.2 \pm 0.2$ $\mu_B$/Co. Following the work of Tiwari *et al.* and Song *et al.* [6] reported successful fabrication of $Ce_{1-x}Co_xO_{2-\delta}$ ($x$ = 0.03) thin films with (111) preferential orientation deposited on a Si (111) substrate by PLD technique. Their deposited films show RT-FM with large magnetic moment of 5.8 $\mu_B$/Co and coercivity of 560 Oe. The authors also showed that the films could be deposited on glass but with smaller magnetic moment and coercivity. These results suggested that the FM in Co-doped $CeO_2$ depend not only on the doping concentration of transition element but also on the microstructure of film, including its crystallization, defects, vacancies, etc.. Vodungbo *et al.* [7] also reported FM in Co-doped $CeO_2$ thin films grown by PLD on $SrTiO_3$ and Si substrate. The films were ferromagnetic with a $T_C$ above 400 K. These authors found that the amount of structural defects had a little effect on FM but the presence of oxygen during the growth or annealing reduced the FM drastically, suggesting that $V_O$ played an important role in the magnetic coupling between Co ions. While Wen *et al.* [10] reported the ferromagnetism observed in undoped and Co-doped $CeO_2$ powders. The RT-FM in undoped $CeO_2$ originated from $V_O$ while a slight Co doping in $CeO_2$ caused a nearly two orders enhancement of saturation magnetization ($M_s$) to 0.47 emu/g compared with the undoped sample. The author suggested that the large RT-FM observed in Co-doped $CeO_2$ powder originated from a combination effect of $V_O$ and Co doping. Similarly, Ou *et al.* [11] reported RT-FM for $Ce_{1-x}Co_xO_2$ ($0 < x < 0.10$) nanorods prepared by electrodeposition route. The nanorods were ferromagnetic with a high $T_C$ about 870 K and the largest $M_s$ of 0.015 emu/g. They suggested that the RT-FM observed in Co-doped $CeO_2$ nanorods adjusted by the structural defects including $V_O$. The same behavior was found in nanoparticles of Fe-doped $CeO_2$ [12] with a $M_s$ value of 0.0062 emu/g in 3 at. % Fe prepared by a sol-gel method, and Fe-doped $CeO_2$ [16] with a $M_s$ value of 0.10 emu/g in 1 at. % Fe prepared by the proteic sol-gel process. The authors suggested that the RT-FM originated from exchange of $F$-center, which involved a combination of $V_O$ and TM doping. However, the source of the magnetism is not only from the magnetically ordered spin of 3D dopants but also from the defects at surface. Ferromagnetic behaviors with large moments were also observed even in undoped $CeO_2$ [17] and $CeO_2$ doped with rare earth such as Nd, Sm [18] or Pr [19]. The authors suggested that defects play an important role in the magnetism, and that only a small fraction of the volume, possibly associated with the surface is active [17-20].

However, magnetic properties of nanospheres of Fe-doped $CeO_2$ have not yet been reported. In this work, we report the ferromagnetism observed in Fe-doped $CeO_2$ nanospheres with particle size of ~100-200 nm synthesized by hydrothermal treatment using polyvinylpyrrolidone (PVP) as a surfactant. The crystallinity and morphology of these samples were characterized by XRD, Raman, and TEM. The valence states of Ce ions and Fe ions were also investigated by XANES, and the magnetic properties of the nanospheres were determined using VSM. The origin of RT-FM in this pure and Fe-doped $CeO_2$ system is also discussed.

## Experimental

In the preparation of monodisperse Fe-doped $CeO_2$ spheres, one gram of PVP was mixed with 40 mL of de-ionized water at room temperature (27℃) until a homogeneous solution was obtained. Subsequently, 3 mmol of $Ce(NO_3)_3{\cdot}6H_2O$ (99.99%, Kento) and $Fe(NO_3)_3{\cdot}9H_2O$ (99.9%, Kanto) were slowly added to the PVP solution to obtain a well-dissolved solution. The homogeneous solution was then transferred into a Teflon-lined stainless steel autoclave of 50 mL capacity and prepared at 200℃ for 12 h. After the autoclave was cooled naturally to room temperature, the precipitate was collected and washed several times with distilled water. The final product was then dried overnight in a vacuum at 80℃. The same procedures were also applied for the preparation of undoped monodisperse $CeO_2$ spheres.

The prepared samples were characterized using XRD, Raman, TEM, XANES, and VSM. A Philips X-ray diffractometer with Cu K$\alpha$ radiation ($\lambda$ = 0.15406 nm) was used to study the phases of the undoped $CeO_2$ and Fe-doped $CeO_2$ samples. Raman spectra were recorded at room temperature using a triple spectrometer (Jobin Yvon/Atago-Bussan T-64000, France). Morphology of the samples was obtained from transmission electron microscopy (TEM, JEOL JEM 2010 200 kV, Japan). High-resolution transmission electron microscopy (HRTEM) was performed using a JEOL JEM 2010 (300 kV, Japan). The Ce $L_3$ edge and Fe $K$ edge XANES spectra were studied using X-ray absorption near-edge structure in transmission mode at the BL8 Station at Siam Photon Laboratory (Synchrotron Light Research Institute (Public Organization), SLRI) in Nakhon Ratchasima, Thailand. The magnetic measurements were performed at room temperature using a vibrating sample magnetometer (VSM 7403, Lakeshore, USA). The magnetic measurements were also performed using quantum design magnetometry (MPMS XL-7, USA) in the zero-field cooling (ZFC) and field cooling (FC) modes with an applied field of 1000 Oe.

## Results and Discussion

### XRD analysis

Figure 1 shows the XRD patterns of the undoped $CeO_2$ and Fe-doped $CeO_2$ prepared at 200℃ for 12 h. All the samples exhibited peaks consistent with the face-centered cubic fluorite structure of $CeO_2$ in the standard data from JCPDS 34-0394 (vertical lines below the patterns). The XRD patterns of the Fe-doped $CeO_2$ are the same as that of undoped $CeO_2$, indicating that Fe ions might have been substituted into the $CeO_2$ lattice, and there are no secondary phases (such as FeO, $Fe_2O_3$, or $Fe_3O_4$) in these samples. The average crystallite sizes of all samples were calculated from X-ray line broadening of the peaks at (111), (200), (220), and (311) planes using Scherrer's equation. There was effect on the sizes of the crystallites with Fe doping (as listed in Table 1). The values of the lattice parameter $a$ of all the samples calculated from the XRD spectra are shown in Table 1. The lattice parameter changed in comparison with undoped $CeO_2$. This change is possibly due to the replacement of larger $Ce^{4+}$ (0.92 Å) by smaller $Fe^{3+}$ (0.65 Å) or $Fe^{2+}$ (0.78 Å), introducing $Ce^{3+}$ into the crystal lattice. $Ce^{3+}$ have a higher ionic radius (1.034 Å) compared to $Ce^{4+}$, and these ions introduce $V_O$. It is observed that $CeO_2$ and Fe-doped $CeO_2$ nanoparticles experience considerable lattice distortion, which is in good agreement with earlier reports [9,13,21]. Those reports indicated that doping causes a change in the Ce-O bond length (lattice distortion) and the overall lattice parameter.

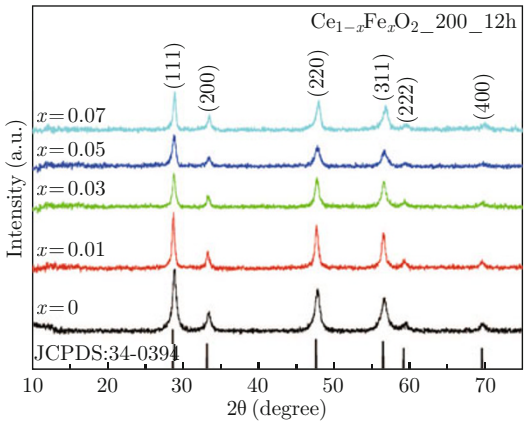


Fig. 1 XRD patterns of undoped $CeO_2$ and Fe-doped $CeO_2$ nanospheres prepared at 200℃ for 12 h.

**Table 1 Summary of crystallite sizes from XRD, Lattice constant, and Magnetization ($M$) of undoped $CeO_2$ and Fe-doped $CeO_2$ nanospheres prepared at 200℃ for 12 h**

| Sample $Ce_{1-x}Fe_xO_2$ | Crystallite size (nm) | Lattice constant, a (nm) | Peak area | Percentage of $Ce^{3+}$ (%) | $M$ at 10 kOe (emu/g) |
|---|---|---|---|---|---|
| $x = 0$ | 19.6 | 0.5420 ± 0.0003 | 5.884 ($Ce^{4+}$)<br>6.095 ($Ce^{4+}$)<br>1.289 ($Ce^{3+}$) | 9.7 | 0.0026 |
| $x = 0.01$ | 18.1 | 0.5423 ± 0.0012 | - | - | 0.0018 |
| $x = 0.03$ | 15.2 | 0.5427 ± 0.0015 | - | - | 0.0058 |
| $x = 0.05$ | 12.7 | 0.5414 ± 0.0018 | 3.160 ($Ce^{4+}$)<br>2.304 ($Ce^{4+}$)<br>1.000 ($Ce^{3+}$) | 15.5 | 0.032 |
| $x = 0.07$ | 14.8 | 0.5406 ± 0.0018 | - | - | 0.027 |

### Raman analysis

The formation of a cubic structure in the Fe-doped $CeO_2$ nanospheres was further supported by Raman spectra. Figure 2 shows typical spectra of Fe-doped $CeO_2$. The peak at about 443-463 $cm^{-1}$ can be assigned to the $F_{2g}$ mode of $CeO_2$, which is the characteristic mode of the Ce-O8 vibrational unit [12]. While the peaks at about 600 $cm^{-1}$ can be assigned to intrinsic $V_O$ (marked with Δ in Fig. 2), which is sensitive to any disorder in the oxygen sublattice resulting from thermal, doping, or grain size [22-25]. The intensity of intrinsic $V_O$ Raman active mode in $Ce_{1-x}Fe_xO_2$ samples is pronounced than in pure $CeO_2$ samples. Such behavior confirms our previous statement that incorporation of Fe ions in $CeO_2$ lattice can be attributed to more $V_O$, especially at $x = 0.2$. In the Raman spectrum of $Ce_{1-x}Fe_xO_2$ nanospheres, the $F_{2g}$ mode is shifted to lower energies with increasing Fe content, which exhibits redshift in this mode [26]. The energy shows redshift of 2, 12, 16, and 19 $cm^{-1}$ for samples with Fe contents of 0.01, 0.03, 0.05, and 0.07, respectively, compared to that of the pure $CeO_2$ nanospheres. This behavior shows the electron molecular vibrational coupling due to increased concentration of substitution of Fe ions in the Ce lattice and the introduction of $V_O$. Beside the $F_{2g}$ and $V_O$ modes, a weak band appears at 210, 277 and 394 $cm^{-1}$ (marked with □ in Fig. 2) observed in $Ce_{1-x}Fe_xO_2$ ($x = 0.2$), which is assigned to hematite ($\alpha$-$Fe_2O_3$) structure. The appearance of

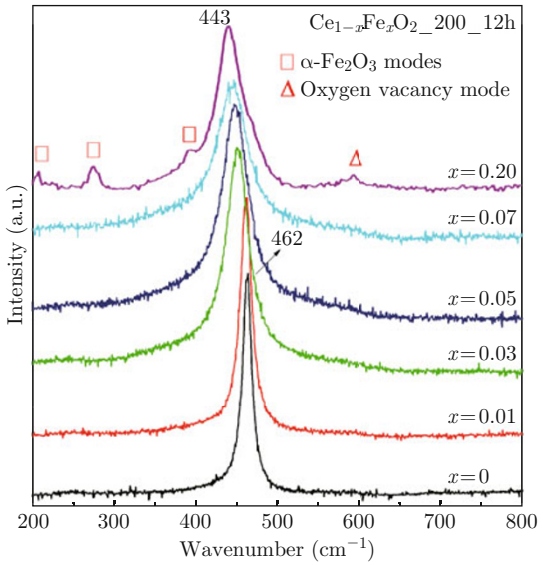


Fig. 2 Raman spectra of undoped $CeO_2$ and Fe-doped $CeO_2$ nanospheres prepared at 200℃ for 12 h.

modes characteristic for hematite structures can be a consequence of impurity phase, implying a possible substitution limit for Fe ions in $CeO_2$.

## TEM analysis

The morphology and structure of Fe-doped $CeO_2$ samples were investigated by TEM as shown in Fig. 3(a)-(e). The TEM bright field images show that the products contain monodisperse nanospheres with a diameter of 100∼200 nm. The average particle size obtained from TEM is larger than the crystallite size obtained from the XRD patterns. This result is similar to the work reported by Zhou *et al.* [27] in which spherical $CeO_2$ crystallites assembled by nanoparticles were formed during hydrothermal treatment, because small nanoparticles of $CeO_2$ aggregated, and gradually evolved into a spherical assemblage to achieve a low surface energy, as shown in Fig. 4. From Fig. 3(b)-(e),

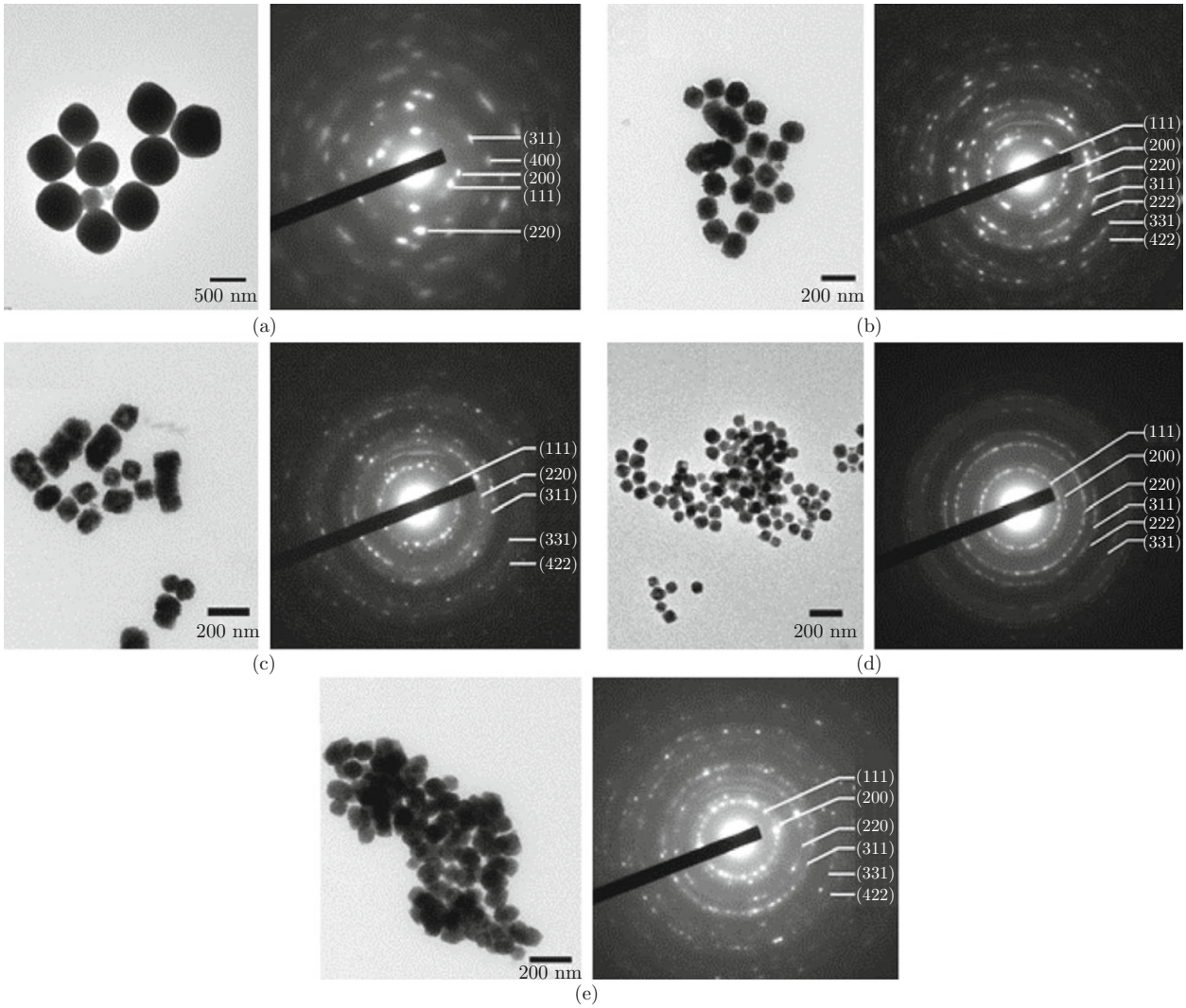


Fig. 3 TEM bright field images with corresponding selected-area electron diffraction (SAED) patterns of Fe-doped $CeO_2$ nanospheres prepared at 200℃ for 12 h for (a) $x = 0$, (b) $x = 0.01$, (c) $x = 0.03$, (d) $x = 0.05$ and (e) $x = 0.07$.

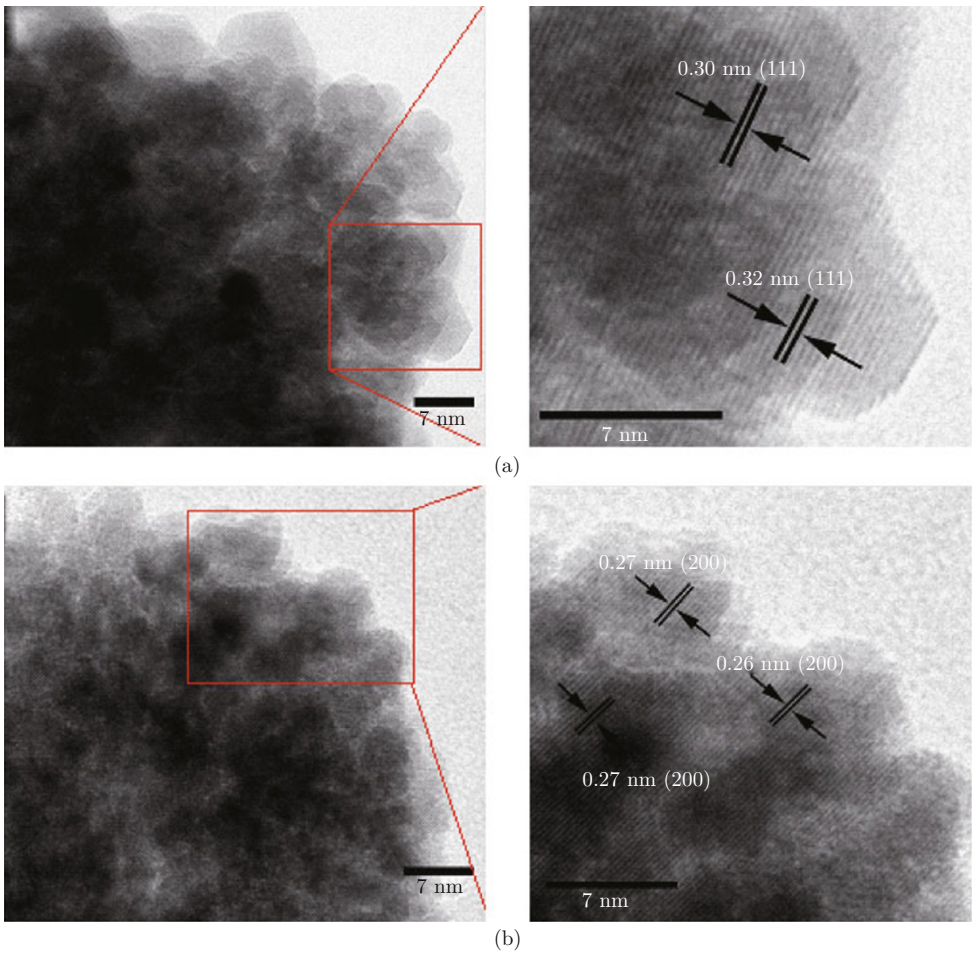


Fig. 4 HRTEM images of Fe-doped $CeO_2$ nanospheres prepared at 200℃ for 12 h for (a) $x = 0.03$, and (b) $x = 0.05$.

morphologies of Fe-doped $CeO_2$ clearly show that nanospheres become smaller as the doped Fe content increases, which agree with the XRD results. It is possible that doping $Fe^{3+}$ can forbid the crystal growth. With higher concentrations of $Fe^{3+}$, it would possibly increase the blockade of crystal growth, giving rise to a decrease in particle size. The same behavior was found in nanoparticles of $TiO_2$ that prohibit the growth in [001] direction after Fe doping as reported by Wen *et al.* [28]. They reported that $Fe^{3+}$ on the surface can form effective pathways for charge interfacial transfer for increasing the photocatalytic activity of $TiO_2$. As a result of this, $Fe^{3+}$ are on the surface of spherical aggregates due to the small particle size, which is beneficial for increasing the magnetic interaction of Fe-doped $CeO_2$ nanospheres. The corresponding selected area electron diffraction (SAED) patterns of the products show spotty ring patterns indicative of a face-centered cubic structure of $CeO_2$ (JCPDS: 34-0394), which is in agreement with the XRD results. HRTEM images of $Ce_{1-x}Fe_xO_2$ for $x = 0.03$ and 0.05, are shown in Fig. 4(a) and 4(b), respectively. The $d$ spacings of the lattice fringes of ~0.30 and 0.32 nm (Fig. 4(a)) calculated from the HRTEM images are corresponding to the (111) plane of $CeO_2$. Similarly, the $d$ spacings of ~0.26 and 0.27 nm (Fig. 4(b)) calculated from the HRTEM images match with (200) plane of $CeO_2$. These are in agreement with the standard data (JCPDS: 34-0394). This result confirms the formation mechanism of Fe-doped $CeO_2$ nanoparticles into nanospheres.

## XANES analysis

The valence state of Ce in undoped $CeO_2$ and Fe-doped $CeO_2$ nanospheres and valence state of Fe were determined by XANES. The XANES spectra at Ce $L_3$ edge were measured in transmission mode, and the Fe $K$ edge XANES spectra of the samples were measured in Fluorescent mode at RT at the BL8 station. Figure 5(a) shows the edge energies of the $CeCl_3$ ($Ce^{3+}$) standard, $CeO_2$ ($Ce^{4+}$) standard, pure $CeO_2$ sample, and $Ce_{1-x}Fe_xO_2$ ($x = 0.05$) sample for comparison. The standard $CeCl_3$ has a single peak illustrated by one intense white line at approximately 5728.8 eV due to the dipole-allowed transition of Ce 2p to Ce $4f^1 5de_g\underline{L}$ final states (represented with $2\underline{p}4f^1 5de_g\underline{L}$, where $\underline{L}$ denotes an oxygen ligand 2p hole); this characterizes the Ce in the $Ce^{3+}$ valence state. In the standard $CeO_2$, all the

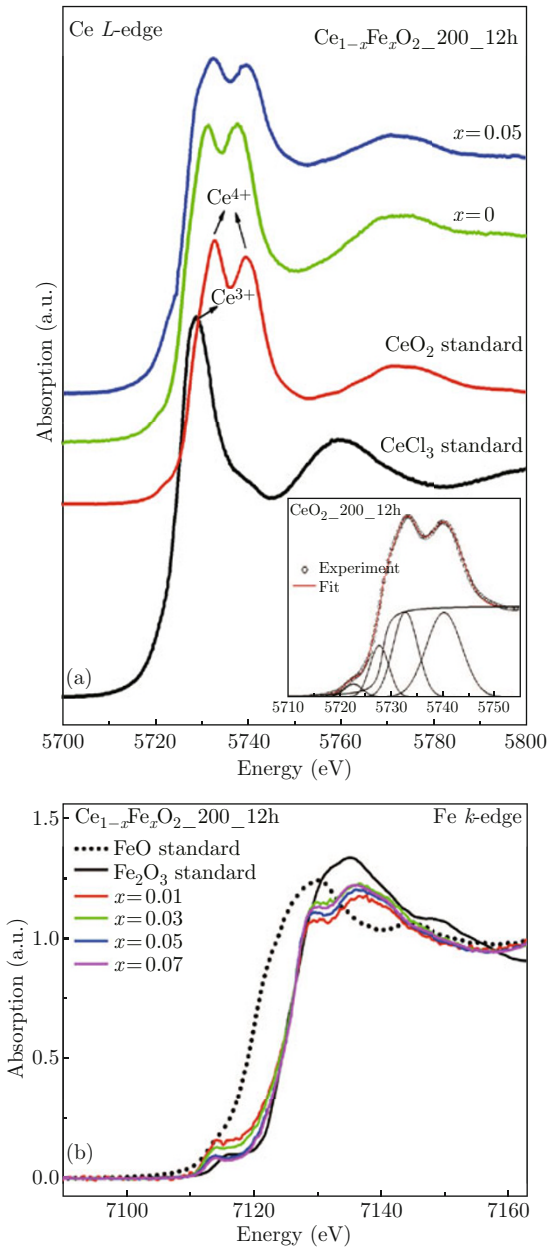


Fig. 5 (a) XANES spectra at the Ce $L_3$ absorption edge for $CeCl_3$, $CeO_2$ standard, and XANES spectra of samples $x = 0$, and $x = 0.05$ at 200℃ for 12 h (Inset shows Gaussian fits of XANES spectra of Ce for samples $x = 0$); (b) XANES spectra at the Fe K absorption edge for FeO ($Fe^{2+}$) standard, $Fe_2O_3$ ($Fe^{3+}$) standard, and XANES spectra of Fe-doped $CeO_2$ nanospheres at 200℃ for 12 h.

spectra are shifted to higher energies, and the white line is split into two peaks with nearly the same intensities at approximately 5732.8 and 5739.8 eV due to an electron excited from Ce 2p to Ce $4f^1 5dt_g\underline{L}$ final states (represented with $2\underline{p}4f^1 5dt_g\underline{L}$) and the excited electron in Ce 4f state and Ce 2p to Ce $4f^0 5d$ final states (represented with $2\underline{p}4f^0 5d$), no electron in the 4f state, respectively, corresponding to the $Ce^{4+}$ valence state [29]. At low energy, the peak of the standard $CeO_2$ is a pre-edge peak, which is assigned to final states of $2\underline{p}5d$ with delocalized d character at the bottom of the conduction band [30, 31]. The three Ce peak positions of all the samples are close to the values of the $CeCl_3$ and $CeO_2$ standards. This result indicates that the Ce ions in our samples are in a mixed valence state of $Ce^{3+}$ and $Ce^{4+}$. The quantitative analysis of the valence state of Ce in each of the three states of Fe-doped $CeO_2$ nanospheres was performed using multi-peak Gaussian fitting obtained from the XANES spectra [32], as shown in inset of Fig. 5(a). The distribution of $Ce^{3+}$ and $Ce^{4+}$ can be obtained by calculation the area ratio of $Ce^{3+}$ and $Ce^{4+}$. The relative concentration of $Ce^{3+}$ are ~9.7% and ~15.5% for undoped $CeO_2$ and Fe-doped $CeO_2$ samples ($x = 0.05$), respectively. It was observed that the percentage of $Ce^{3+}$ of the $Ce_{1-x}Fe_xO_2$ samples ($x = 0.05$) is higher than those of undoped $CeO_2$ samples because of the incorporation of Fe. The percentage of $Ce^{3+}$ is ~15.5% in Fe doped, which is lower than those of 21.5% in the $Ce_{1-x}Fe_xO_2$ samples ($x = 0.1$) reported by Wang *et al.* [33] Their result was calculated based on X-ray photoelectron spectroscopy (XPS), which more sensitive to surface.

Figure 5(b) shows the edge energies of the FeO ($Fe^{2+}$) standard, $Fe_2O_3$($Fe^{3+}$) standard, and Fe-doped $CeO_2$ samples at different concentrations prepared at 200℃ for 12 h for comparison. The shift of the edge position can be used to determine the valence state. From Fig. 5(b), edge position of FeO ($Fe^{2+}$) standard is approximately 7120 eV, while $Fe_2O_3$ ($Fe^{3+}$) standard is approximately 7125 eV. These can be used simply as a fingerprint of phases and valence state. It is seen that the edge positions of all the samples were quite similar to those of the $Fe_2O_3$ standard at approximately 7125 eV. In addition, the feature of all samples was very similar in terms of shape and position to the $Fe_2O_3$ standard at approximately 7128 and 7134 eV, respectively. Thus, this result indicates that most of the Fe ions in our samples are in the $Fe^{3+}$ valence state. These spectra at the Fe *K* edge are very similar to those of the Fe from aerosols samples reported by Ohta *et al.* [34] showing a pre-edge feature approximately 7114 eV due to an electron excited from the Fe 1s to the Fe 3D final states.

## Magnetic properties

Figure 6 shows the field dependence of the specific magnetization (*M-H* curve) of undoped $CeO_2$ and Fe-doped $CeO_2$ samples, obtained from VSM measurements at RT. The magnetic component corresponding to the samples holder was subtracted from all the presented data. The samples show weak RT-FM and the $M_S$ increases with increasing Fe concentration. The highest $M_S$ was observed for $x = 0.05$ with value of approximately 0.03 emu/g at 10 kOe. The magnetizations of the Fe-doped $CeO_2$ samples for $x = 0.07$ have both FM and paramagnetism (PM) increasing with an

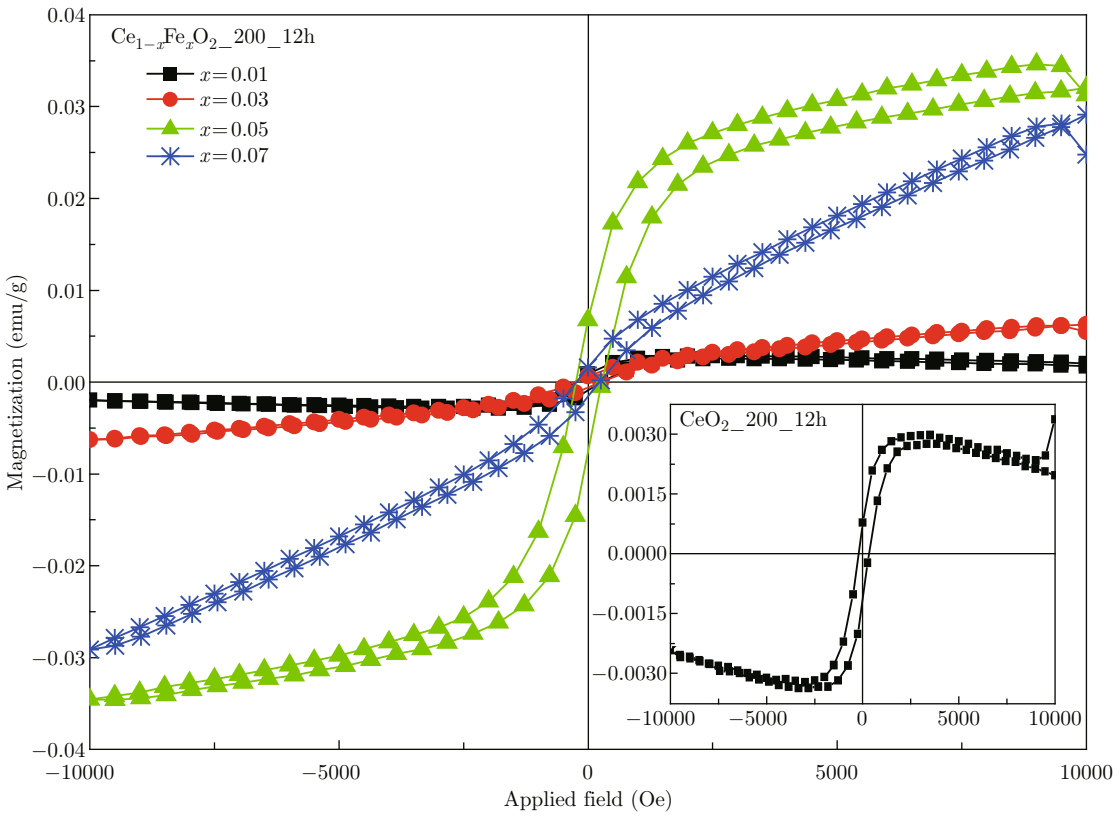


Fig. 6 Magnetic properties of Fe-doped $CeO_2$ nanospheres prepared at 200°C for 12 h (inset shows magnetic loop of undoped $CeO_2$).

increasing magnetic field. The $M$ values of all the samples are shown in Table 1. In comparison to other works, the $M_S$ value of 0.03 emu/g in this work is lower than the reported $M_S$ values for Fe-doped $CeO_2$ powders at $x = 0.01$ (0.1 emu/g at 45 kOe) [12] and Fe-doped $CeO_2$ pellets at $x = 0.05$ (0.24 emu/g at 10 kOe) [35]. However, the $M_S$ value in our result is higher than those of other reports, i.e., Fe-doped $CeO_2$ nanocrystals at $x = 0.03$ (0.0062 emu/g at 10 kOe) [16] and Fe-doped $CeO_2$ nanocrystals at $x = 0.12$ (0.02 emu/g at 0.6 kOe) [26]. The difference in $M_S$ in the magnetic properties of Fe-doped $CeO_2$ materials depends on the preparation conditions such as temperature and atmosphere [36,37]. We also observed RT-FM in undoped $CeO_2$ nanospheres with $M_S$ of approximately 0.0026 emu/g at 10 kOe. This result is interesting because bulk $CeO_2$ is an insulator with $Ce^{4+}$ in the $4f^0$ configuration. Generally, magnetic ordering in insulating oxides is antiferromagnetic ordering due to the superexchange coupling, but $CeO_2$ is often used as a storage medium because a $V_O$ can easily be formed in $CeO_2$. Similar results have been obtained in some other work [17,21]. Sundaresan *et al.* [21] reported that the weak ferromagnetism, with $M_S$ of approximately 0.0019 emu/g at 5 kOe in pure $CeO_2$ nanoparticles (average size of 15 nm) as well as in other undoped oxide semiconductors, results from the exchange interactions between electron spin moment of $Ce^{3+}$ and the $V_O$ at the particle surface. This direct ferromagnetic coupling is called the $F$-center exchange (FCE) [13,38,40]. It is possible that $V_O$ can create magnetic moments on neighboring Ce-ions of $Ce^{3+}$-$\nabla$-$Ce^{3+}$, where $\nabla$ denotes a $V_O$.

For explanation the origin of the ferromagnetic contribution in Fe ions-doped $CeO_2$ nanospheres, the following arguments are proposed. First, the ferromagnetic behavior is associated with FCE coupling, in which both $V_O$ and Fe ions are involved. In this work, the XANES spectra show evidence of $Fe^{3+}$ substitution in $CeO_2$, and the Ce ions of 3+ state (with $4f^1$ configuration), which can be attributed to $V_O$ in Fe-doped $CeO_2$ samples. Therefore, the RT-FM in these samples was suggested according to the FCE of $Fe^{3+}$-$\nabla$-$Fe^{3+}$ complex in the structure. This FCE forms bound magnetic polarons (BMP) and neighboring BMPs can overlap and result in the long-range Fe-Fe ferromagnetic coupling in $CeO_2$. The radius of the electron trapped orbital, that overlaps the $d$ shells of both Fe ion neighbors, is of the order $a_0\varepsilon$, where $a_0$ is the Bohr radius, and $\varepsilon$ is the dielectric constant of the material. In $CeO_2$ ($\varepsilon = 26$), the radius of the $F$-electron orbital is estimated to be ~14 Å [5], which is required for a long-range FM order. As $Fe^{3+}$ ($3D^5$) ions in the case of low-spin state only have unoccupied minority spin orbitals [40], the trapped electron in vacancy will be ↓

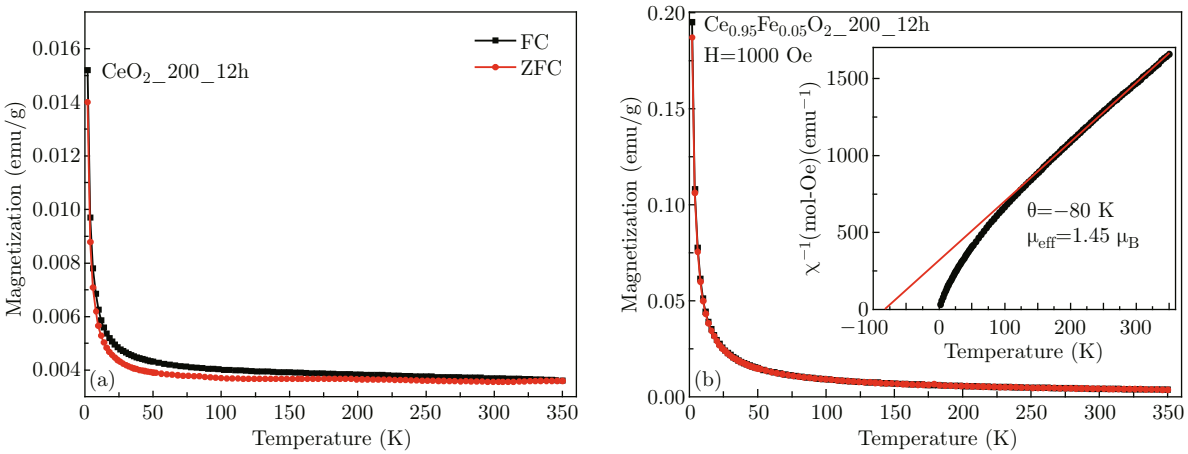


Fig. 7 $M$-$T$ curves at 1 kOe of samples nanospheres prepared at 200℃ for 12 h (a) Undoped $CeO_2$ and (b) Fe-doped $CeO_2$ ($x = 0.05$). Inset exhibits the Curie-Weiss behavior of the inverse susceptibility for Fe-doped $CeO_2$ ($x = 0.05$).

and the two Fe neighbors ↑, according to the Hund's rule and Pauli Exclusion Principle. Second, the double exchange interaction is investigated. It is coupling between nearest neighbor of Fe ions with different valence and oxygen ions ($Fe^{2+}$-$O^{2-}$-$Fe^{3+}$). However, mechanism of ferromagnetism on this interaction cannot produce long-range magnetic order because of concentrations of Fe ions of a few percent in structure. Moreover, the XANES results in Fe-doped $CeO_2$ showed that no mixed of Fe ions exist. Finally, ferromagnetism may originated by Fe clusters. If Fe cluster exist the magnetic moment would be proportional to the amount of Fe concentration but no tendency in our $M$ results observed. Therefore, the RT-FM in these samples, and the exchange interaction between Vo and the surrounding of $Fe^{3+}$ was suggested as being a result of the FM according to the FCE.

It is observed that the loss of $M$ induced by Fe-doped at $x = 0.01$ compared to undoped $CeO_2$. This case is due to the pairing of the electron clouds surrounding $V_O$, which are electron excess left behind in the vacancies [41]. With high concentrations of Fe ions, it would possibly increase the amount of magnetic moments and enhance significantly in ferromagnetism. Moreover, the additional exchange interactions between the spins of the $Ce^{3+}$ are responsible for the observed enhanced ferromagnetism in these samples. At higher Fe concentrations ($x = 0.07$) in our case, Fe ions become closer together as the Fe content increases, which increases the superexchange interactions between these neighboring Fe ions of $Fe^{3+}$-$O^{2-}$-$Fe^{3+}$ gives rise to an antiferromagnetic behavior. As a result of this, the ferromagnetism decreases in the average magnetic moment per Fe ion and appears to be a paramagnetic effect. However, the exact mechanism for different magnetizations of Fe-doped $CeO_2$ samples with different Fe concentrations is still unclear, and further work is needed.

The temperature dependence of magnetization ($M$ – $T$ curve) of undoped $CeO_2$ and Fe-doped $CeO_2$ ($x = 0.05$) samples were measured under $H$ of 1 kOe in the zero field cooling (ZFC) and field cooling (FC) modes as shown in Fig. 7. The ZFC-FC curves showed similar behavior of each sample and no evidence of secondary phase was existed down to 2 K. The $Tc$ or Neel temperatures ($T_N$) in these samples do not match to those values of Fe ($T_C$ ~1043 K), FeO ($T_N$ ~200 K), $\alpha$-$Fe_2O_3$ ($T_C$ ~240 K), or $Fe_3O_4$ ($T_C$ ~858 K) [42]. From PM component in Fe-doped $CeO_2$ samples, the paramagnetic region can be well fitted using a simple Curie-Weiss equation, $\chi = C/(T-\theta)$ where $\chi$ is susceptibility, $C$ is the Curie constant, $T$ and $\theta$ are experimental temperature and the Curie-Weiss temperature, respectively. The linear plot of inverse $\chi$ dependence of the temperature is shown in the inset of Fig. 7(b). It exhibited a good fit obtained at high temperature for Fe-doped $CeO_2$ samples, except in undoped $CeO_2$. The sample had a negative value of $\theta$ (~-80 K), which indicates antiferromagnetic interactions between Fe ions. This behavior can be described using the Curie-Weiss equation with the effective magnetic moments of $\mu_{eff}$ ≈1.45 $\mu_B$ for Fe-doped $CeO_2$. This is close to that of the low-spin state of $Fe^{3+}$ ion ($\mu_{eff}$ = 1.73 $\mu_B$). These effective magnetic moments correspond to the free $Fe^{3+}$ without magnetic interactions or PM defect in the system.

## Conclusions

Nanospheres of undoped $CeO_2$ and Fe-doped $CeO_2$ have been successfully synthesized by a hydrothermal method using PVP as a surfactant. The XRD and SEAD results indicated that all the samples had a face-centered cubic structure and that no secondary phase was detected, which indicated that $Fe^{3+}$ ions were substituted in $Ce^{4+}$ sites. $Fe^{3+}$ doping causes redshift of

the $F_{2g}$ Raman mode due to the increased concentration of $Ce^{3+}$ with oxygen vacancies. The oxygen vacancy is confirmed by XANES measurements, which reveals that most of the Fe ions are in the 3+ state, and that some Ce ions transform to the 3+ state. The $Ce^{3+}$ and $Fe^{3+}$ spin electrons are induced weak RT-FM. This behavior indicated that the ferromagnetism is essentially related to oxygen vacancy/defects.

## Acknowledgements

The authors would like to thank the Synchrotron Light Research Institute (Public Organization), Nakhon Ratchasima, Thailand for XANES facilities, and Clarendon Laboratory, Department of Physics, University of Oxford, United Kingdom for quantum design magnetometry facilities. S. Phokha would like to acknowledge the financial support for her Ph.D. studies from the Thailand Research Fund through the Royal Golden Jubilee Ph.D. program (Grant No. PHD/0275/2550). This work was supported by Suranaree University of Technology (SUT) and by the Office of the Higher Education Commission under NRU project of Thailand.

## References

[1] T. Dietl, H. Ohno, F. Matsukura, J. Cibert and D. Ferrand, "Zener model description of ferromagnetism in zinc-blende magnetic semiconductors", Science 287(5455), 1019-1022 (2000). http://dx.doi.org/10.1126/science.287.5455.1019

[2] S. J. Pearton, W. H. Heo, M. Ivill, D. P. Norton and T. Steiner, "Dilute magnetic semiconducting oxides", Semicond. Sci. Technol. 19(10), R59 (2004). http://dx.doi.org/10.1088/0268-1242/19/10/R01

[3] N. H. Hong, J. Sakai, N. Poirot and V. Brize, "Room-temperature ferromagnetism observed in undoped semiconducting and insulating oxide thin films", Phys. Rev. B 73(13), 132404 (2006). http://dx.doi.org/10.1103/PhysRevB.73.132404

[4] X. Chen, G. Li, Y. Su, X. Qui, L. Li and Z. Zou, "Synthesis and room-temperature ferromagnetism of $CeO_2$ nanocrystals with nonmagnetic $Ca^{2+}$ doping", Nanotechnology 20(11), 115606 (2009). http://dx.doi.org/10.1088/0957-4484/20/11/115606

[5] A. Tiwari, V. M. Bhosle, S. Ramachandran, N. Sudhakar, J. Narayan, S. Budak and A. Gupta, "Ferromagnetism in Co doped $CeO_2$: Observation of a giant magnetic moment with a high Curie temperature", Appl. Phys. Lett. 88(14), 142511 (2006). http://dx.doi.org/10.1063/1.2193431

[6] Y. Q. Song, H. W. Zhang, Q. Y. Wen, Y. X. Li and J. Q. Xiao, "Room-temperature ferromagnetism of co-doped $CeO_2$ thin films on si(111) substrates", Chin. Phys. Lett. 24(1), 218-221 (2007). http://dx.doi.org/10.1088/0256-307X/24/1/059

[7] B. Vodungbo, Y. Zheng, F. Vidal, D. Demaille, V. H. Etgens and D. H. Mosca, "Room temperature ferromagnetism of Co doped $CeO_{2-\delta}$ diluted magnetic oxide: Effect of oxygen and anisotropy", Appl. Phys. Lett. 90(6), 062510 (2007). http://dx.doi.org/10.1063/1.2472520

[8] V. Fernandes, J. J. Klein, N. Mattoso, D. H. Mosca, E. Silveira, E. Ribeiro, W. H. Schreiner, J. Varalda and A. J. A. de Oliveira, "Room temperature ferromagnetism in Co-doped $CeO_2$ films on Si(001)", Phys. Rev. B 75(12), 121304R (2007). http://dx.doi.org/10.1103/PhysRevB.75.121304

[9] A. Thurber, K. M. Reddy, V. Shutthanandan, M. H. Engelhard, C. Wang, J. Hays and Punnoose, "Ferromagnetism in chemically synthesized $CeO_2$ nanoparticles by Ni doping", Phys. Rev. B 76(16), 165206 (2007). http://dx.doi.org/10.1103/PhysRevB.76.165206

[10] Q. Y. Wen, H. W. Zhang, Y. Q. Song, Q. H. Yang, H. Zhu and J. Q. Xiao, "Room-temperature ferromagnetism in pure and Co doped $CeO_2$ powders", J. Phys.: Condens. Mat. 19(24), 246205 (2007). http://dx.doi.org/10.1088/0953-8984/19/24/246205

[11] Y. N. Ou, G. R. Li, J. H. Liang, Z. P. Feng and Y. X. Tong, "$Ce_{1-x}Co_xO_{2-\delta}$ nanorods grown by electrochemical deposition and their magnetic properties", J. Phys. Chem. C 114(32), 13509-13514 (2010). http://dx.doi.org/10.1021/jp1038128

[12] P. C. A. Brito, D. A. A. Santos, J. G. S. Duque and M. A. M. Macedo, "Structural and magnetic study of Fe-doped $CeO_2$", Physica B 405(7), 1821-1825 (2010). http://dx.doi.org/10.1016/j.physb.2010.01.054

[13] M. Y. Ge, H. Wang, E. Z. Liu, J. F. Liu, J. Z. Jiang, Y. K. Li, Z. A. Xu and H. Y. Li, "On the origin of ferromagnetism in $CeO_2$ nanocubes", Appl. Phys. Lett. 93, 062505 (2008). http://dx.doi.org/10.1063/1.2972118

[14] S. Kumar, Y. J. Kim, B. H. Koo, and C. G. Lee and J. Nanosci. "Structural and magnetic properties of Ni doped $CeO_2$ nanoparticles", J. Nanosci. Nanotechnol. 10(11), 7204-7207 (2010). http://dx.doi.org/10.1166/jnn.2010.2751

[15] P. O. Maksimchuk, A. A. Masalov, Yu.V. Malyukin, "Spectroscopically detected formation of oxygen vacancies in nano-crystalline $CeO_{2-x}$", J. Nano-Electron. Phys. 5(1), 01004 (2013).

[16] S. Maensiri, S. Phokha, P. Laokul, and S. Seraphin, "Room temperature ferromagnetism in Fe-doped $CeO_2$ nanoparticles", J. Nanosci. Nanotechnol. 9(11), 6415-6420 (2009). http://dx.doi.org/10.1166/jnn.2009.1372

[17] S. Phokha, S. Pinitsoontorn, P. Chirawatkul, Y. Poo-arporn and S. Maensiri, "Synthesis, characterization, and magnetic properties of monodisperse $CeO_2$ nanospheres prepared by PVP-assisted hydrothermal method", Nanoscale Res. Lett. 7, 425 (2012). http://dx.doi.org/10.1186/1556-276X-7-425

[18] M. C. Dimri, H. Khanduri, H. Kooskora, J. Subbi, I. Heinmaa, A. Mere, J. Krustok and R. Stern, "Ferro-

magnetism in rare earth doped cerium oxide bulk samples", Phys. Status Solidi A 209(2), 353-358 (2012). http://dx.doi.org/10.1002/pssa.201127403

[19] N. Paunović Z. D. Mitrović R. Scurtu, S. Aškrabić M. Prekajski, B. Matović and Z. V. Popović "Suppression of inherent ferromagnetism in Pr-doped $CeO_2$ nanocrystals", Nanoscale, 4(17), 5469-5476 (2012). http://dx.doi.org/10.1039/c2nr30799e

[20] K. Ackland, L. M. A. Monzon, M. Venkatesan and J. M. D. Coey, "Magnetism of Nanostructured $CeO_2$", IEEE Trans. Magn. 47(10), 3509-3512 (2011). http://dx.doi.org/10.1109/TMAG.2011.2150743

[21] A. Sundaresan, R. Bhargavi, N. Rangarajan, U. Siddesh and C. N. R. Rao, "Ferromagnetism as a universal feature of nanoparticles of the otherwise nonmagnetic oxides", Phys. Rev. B 74(16), 161306(R) (2006).

[22] S. Maensiri, C. Marsingboon, P. Loakul, W. Jareonboon, V. Promarak, P. L. Anderson and S. Seraphin, "Egg white synthesis and photoluminescence of platelike clusters of $CeO_2$ nanoparticles", Cryst. Growth. Des. 7(5), 950-955 (2007). http://dx.doi.org/10.1021/cg0608864

[23] S. Phoka, P. Laokul, E. Swatsitang, V. Promarak, S. Seraphinc and S. Maensiri, "Synthesis, structural and optical properties of $CeO_2$ nanoparticles synthesized by a simple polyvinyl pyrrolidone (PVP) solution route", Mater. Chem. Phys. 115(1), 423-428 (2009). http://dx.doi.org/10.1016/j.matchemphys.2008.12.031

[24] I. Kosacki, T. Suzuki, V. Petrovsky, H. U. Anderson and Ph. Colomban, "Raman scattering and lattice defects in nanocrystalline $CeO_2$ thin films", Solid State Ionics 149(1-2), 99-105 (2002).

[25] I. Kosacki, V. Petrovsky, H. U. Anderson and Ph. Colomban, "Raman spectroscopy of nanocrystalline ceria and zirconia thin films", J. Am. Ceram. Soc. 85(11), 2646-2650 (2002). http://dx.doi.org/10.1111/j.1151-2916.2002.tb00509.x

[26] Z. D. Dohcevic-Mitrovic, N. Paunovic, M. Radovic, Z. V. Popovic, B. Matovic, B. Cekic and V. Ivanovski, "Valence state dependent room-temperature ferromagnetism in Fe-doped ceria nanocrystals", Appl. Phys. Lett. 96(20), 203104 (2010). http://dx.doi.org/10.1063/1.3431581

[27] F. Zhou, X. Ni, Y. Zhang and H. Zheng, "Size-controlled synthesis and electrochemical characterization of spherical $CeO_2$ crystallites", J. Colloid Interf. Sci. 307(1), 135-138 (2007). http://dx.doi.org/10.1016/j.jcis.2006.11.005

[28] L. Wen, B. Liu, X. Zhao, K. Nakata, T. Murakami and A. Fujishima, "Synthesis, characterization, and photocatalysis of Fe-doped $TiO_2$: A combined experimental and theoretical study", Int. J. Photoenergy 2012, 368750 (2012). http://dx.doi.org/10.1155/2012/368750

[29] J. Hormes, M. Pantelouris, G.B. Balazs and B. Rambabu, "X-ray absorption near edge structure (XANES) measurements of ceria-based solid electrolytes", Solid State Ionics 136-137, 945-954 (2000). http://dx.doi.org/10.1016/S0167-2738(00)00533-6

[30] F. Zhang, P. Wang, J. Koberstein, S. Khalid and S. W. Chan, "Cerium oxidation state in ceria nanoparticles studied with X-ray photoelectron spectroscopy and absorption near edge spectroscopy", Surf. Sci. 563(1-3), 78-82 (2004). http://dx.doi.org/10.1016/j.susc.2004.05.138

[31] J. Zhang, Z. Wu, T. Liu, T. Hu, Z. Wu and X. Ju, "XANES study on the valence transitions in cerium oxide nanoparticles", J. Synchrotron Radiat. 8, 531-532 (2001). http://dx.doi.org/10.1107/S0909049500016022

[32] C. Wan, X. Ju, Y. Qi, Y. Zhang, S. Wang. X. Liu and L. Jiang, "Synchrotron XRD and XANES studies of cerium-doped $NaAlH_4$: Elucidation of doping induced structure changes and electronic state", J. Alloy. Compd. 481(1-2), 60-64 (2009). http://dx.doi.org/10.1016/j.jallcom.2009.03.128

[33] J. Wang, B. Zhang, M. Shen, J. Wang, W. Wang, J. Ma, S. Liu and L. Jia, "Effects of Fe-doping of ceria-based materials on their microstructural and dynamic oxygen storage and release properties", J. Sol-Gel Sci. Techn. 58(1), 259-268 (2011). http://dx.doi.org/10.1007/s10971-010-2386-3

[34] A. Ohta, H. Tsuno, H. Kagi, Y. Kanai, M. Nomura, R. Zhang, S. Terashima and N. Imai, "Chemical compositions and XANES speciations of Fe, Mn and Zn from aerosols collected in China and Japan during dust events", Geochem. J. 40(4), 363-376 (2006). http://dx.doi.org/10.2343/geochemj.40.363

[35] R. K. Singhal, P. Kumari, S. Kumar, S. N. Dolia, Y. T. Xing, M. Alzamora, U. P. Deshpande, T. Shripathi and E. Saitovitch, "Room temperature ferromagnetism in pure and Co- and Fe-doped $CeO_2$ dilute magnetic oxide: Effect of oxygen vacancies and cation valence", J. Phys. D: Appl. Phys. 44(16), 165002 (2011). http://dx.doi.org/10.1088/0022-3727/44/16/165002

[36] S. Maensiri, S. Phokha, P. Laokul and S. Seraphin, "Room temperature ferromagnetism in Fe-Doped $CeO_2$ nanoparticles", J. Nanosci. Nanotechnology 9(11), 6415-6420 (2009).

[37] J. M. D. Coey, M. Venkatesan and C. B. Fitzerald, "Donor impurity band exchange in dilute ferromagnetic oxides", Nat. Mater. 4(2), 173-179 (2005). http://dx.doi.org/10.1038/nmat1310

[38] V. Fernandes, R. J. O. Mossanek, P. Schio, J. J. Klein, A. J. A. de Oliveira, W. A. Ortiz, N. Mattoso, J. Varalda, W. H. Schreiner, M. Abbate and D. H. Mosca, "Dilute-defect magnetism: Origin of magnetism in nanocrystalline $CeO_2$", Phys. Rev. B 80(3), 035202 (2009). http://dx.doi.org/10.1103/PhysRevB.80.035202

[39] J. M. D. Coey, A. P. Douvalis, C. B. Fitzgerald and M. Venkatesan, "Ferromagnetism in Fe-doped $SnO_2$ thin films", Appl. Phys. Lett. 84(8), 1332-1334 (2004). http://dx.doi.org/10.1063/1.1650041

[40] F. Esch, S. Fabris, L. Zhou, T. Montini, C. Africh, P. Fornasiero, G. Comelli and R. Rosei, "Electron localization determines defect formation on ceria substrates", Science, 309(5735), 752-755 (2005). http://dx.doi.org/10.1126/science.1111568

[41] M. Radovic, Z. Dohcevic-Mitrovic, N. Paunovic, M. Scepanovic, B. Matovic and Z. V. Popovic, "Hydrothermal synthesis of $CeO_2$ and $Ce_{0.9}Fe_{0.1}O_2$ nanocrystals", Acta Phys. Pol. A 116(4), 614-617 (2009).

[42] V. Fernandes, P. Schio, A. J. A. de. Oliveira, W. H. Schreiner, and J. Varalda and D. H. Mosca, "Loss of magnetization induced by doping in $CeO_2$ films", J. Appl. Phys. 110(11), 113902 (2011). http://dx.doi.org/10.1063/1.3664764

[43] S. Colis, A. Bouaine, G. Schmerber, C. Ulhaq-Bouillet, A. Dinia, S. Choua and P. Turek, "High-temperature ferromagnetism in Co-doped $CeO_2$ synthesized by the coprecipitation technique", Phys. Chem. Chem. Phys. 14(20), 7256-7263 (2012). http://dx.doi.org/10.1039/c2cp23973f